18th International Conference on Protection & Automation in Power System
Shahrood University of Technology
January 9, 2024 - January 10, 2024

Controllable DC Saturated Core Fault Current Limiter with Loss Reduction

Alireza Rezapoor-Barabady
Ali A. Razi-Kazemi
Sadegh Mohsenzade
Electrical Engineering Department
K. N. Toosi University of Technology
Tehran, Iran
a.rezapoorbarabady@email.kntu.ac.ir
razi.kazemi@kntu.ac.ir
s.mohsenzade@kntu.ac.ir

Alireza Tabatabaei Malazi
Alireza Jafari
Electrical Engineering Department
K. N. Toosi University of Technology
Tehran, Iran
a.tabatabaeimalazi@email.kntu.ac.ir
a.jafari@email.kntu.ac.ir

***Abstract*—Because of the increased fault current rate and lack of zero current in DC networks like rail transport lines, using fault current limiters (FCL) necessitated a different topology for network elements. FCLs based on core saturation have less of an impact on the network and are less flexible when it comes to handling different kinds of faults because they can not be controlled in terms of time when lowering the fault current. Some FCLs are not time-controllable and have losses in the network before the fault. These factors contribute to their shortcomings. This paper investigates on fast-response FCLs using permanent magnets(PM) and core saturation. These FCLs can control the time of fault current reduction during DC circuit breaker (DCCB) operation, also it is possible to reduce the amount of fault current, which is one of the critical fault parameters, by adding control modes that include two control coils and their drive circuit. The time setting is done to observe the most significant effect at the moment of the fault (DCCB operation). At last, by adjusting the voltage and control coils turn number, in addition to reduce the number of turns of the main coil connected to the network, which causes a reduction in the impedance of the path (reduction of losses) before the fault, have time control on the fault current rate. The fault current limiter designed in the desired DC network is validated by using the finite element simulation method in Ansys Maxwell software.**

Keywords— Fault current limiters, Magnetic coupling, DC circuit breaker, Controllable FCL, DC transmission line

I. Introduction

With the progress and improvement of DC networks based on different topologies[1], the need to increase the capacity and also the speed of DCCB operation has increased more than in the past [2]. According to the characteristics of the structure of DC networks, in addition to the large fault current amplitude[3], also the increment rate of fault current is also very significant [4]. Since DC switches have high sensitivity [5], they should have the least stress for successful interruption.

The existing switches that are commonly used in DC networks are mechanical [6], hybrid switches [7], and solid-state switches [8].

Mechanical switches use the resonant circuit mechanism to interrupt the current [8], and usually, their interruption time is a few tens of milliseconds. These types of switches are limited in interrupting high currents. Solid state switches use control devices such as IGBT blocks to interrupt the fault current more quickly but have higher losses than mechanical switches [9]. Hybrid switches structure comprised the previous two switches, including the main flow branch, the flow cut branch by IGBTs, and the energy absorption branch (arrester), which are very expensive to make these switches [10].

According to what was said, the cost of a DC breaker with the ability to interrupt high transient currents is very high [11]. Also, with the increase of the fault current level, the fault current increment rate will be upward, as a result, the DC breaker is depreciated under the stress of current interruption and in case of successful disconnection its life span is reduced [12]. Also, there are limitations in the construction and dimensions of DC

breakers. Therefore, DC fault current limiters are used to limit DC switches in interrupting high fault current and its high rate [11].

Although in the past, series reactors were used to limit the fault, however in the transient state the effect was minimal and caused high losses in the network in pre-fault [13].

FCLs are divided into four main categories: FCLs based on superconductors, FCLs based on semiconductor devices, hybrid FCLs, and FCLs with a special core structure [14].

In superconductors, the superconducting element is placed as a variable resistance directly or through magnetic coupling in the network circuit. The advantage of this model is the high speed of operation during the fault, but the high cost of construction and the complex cooling system [15]. Also, very large dimensions in construction are one of the problems of this model [16].

Semiconductor FCLs also consist of two coils, one in the network and the other connected to the semiconductor switches. The secondary coil has the task of saturating the magnetic core, which is connected to a DC converter, by creating a magnetic flux opposite to the winding flux. It leads the main screw connected to the core grid to the saturation area[17]. One of the advantages of these FCLs is the high speed, while the losses of the converter to saturate the core and also the resistance of the semiconductors in the operation state are very high [17].

Hybrid FCLs have smaller dimensions than superconductors and fewer losses than semiconductors. This model is composed of the combination of both mentioned current limiters. The complexity of the structure of these FCLs is one of their main problems [18].

FCLs with a special core structure are based on core saturation. Most of these FCLs have a core that consists of two parts. The core contains one or more soft magnetic materials and a permanent magnet to saturate the core. The permanent magnet causes the core to saturate in pre-fault and when the fault occurs, the network coil creates a flux opposite to the flux of the permanent magnet in the core, which brings the core out of saturation and the impedance of the path increases. The positive point of this structure is its low electrical losses [19]. The impedance in the network winding and the amount of current reduction depends on the amount of short-circuit current in the fault condition. Lack of time controllability is one of the disadvantages of this model [20].

In the FCLs with a special core structure called controllable saturated core fault current limiter (CSCFCL), by adding two control coils with circuits connected to voltage sources that can be controlled by IGBT blocks, a controllable FCL has been presented. In the pre-fault state, the core structure saturates by PM. As the fault occurs, the flux of network winding and second control winding makes the core unsaturate and the inductance increases. While the core is saturated again, the third coil enters and makes the core unsaturated. As a result, the impedance remains at its maximum state for a longer period and the fault current decreases for more extended period. The most important features compared to other similar FCLs are controllability and time flexibility, fast- response to the fault

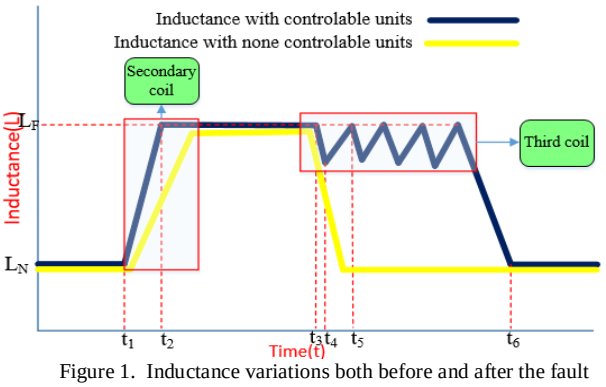

Figure 1. Inductance variations both before and after the fault

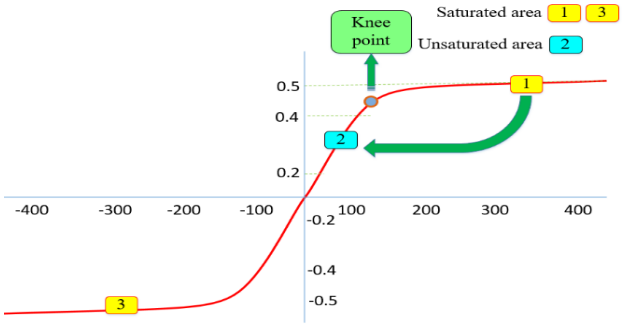

Figure 2. B-H curve of core

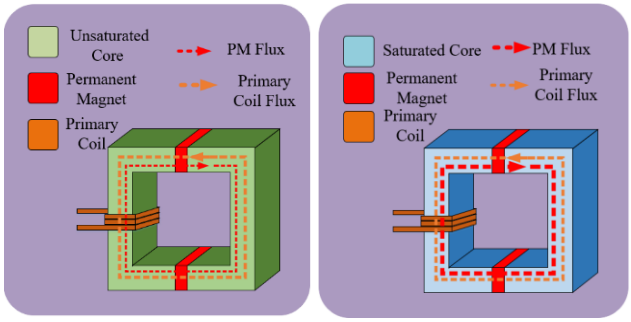

Figure 3. (a)unsaturated core (b) saturated core

and much less loss by reducing the number of turns of the network coil before the fault. In this article, it was tried to analyze the sensitivity of the proposed structure to the voltage level connected to the coils.

II. Principle of PMBASE FCL

FCLs that are based on core saturation through pm are composed of three main parts: PM, an integrated core of one or more soft magnetic materials such as ferrite or silicon steel and a copper coil connected to the grid.

In these FCLs, according to Fig. 3, in the pre-fault, the core goes to saturation through the permanent magnet. In this case, according to the B-H curve of the magnetic material that makes up the core, the core is at point 1 as shown in Fig. 1. At this

point, the nominal current flowing through the network coil produces a flux that is larger than the flux produced by PM. As a result, the impedance value at point 1 will decrease since the inductance is at its lowest magnitude according to (3), which is directly correlated with the slope of the B-H curve (the magnetic permeability coefficient of the core).

When the fault occurs and the current increases the flux produced by the coil overcomes the flux created by PM and moves the operation point of the core in the B-H curve to point 2 in the linear region of the core. At point 2, the slope of the B-H curve is much greater than μ_r to point 1 will cause the inductance to increase and the slope of the fault current to decrease transiently according to (1). Then the DC breaker can perform the disconnection operation with a lower current stress.

The quantity of fault current and the time it takes to increase the fault current rate determine how far the core's stationary point moves on the B-H curve. This displacement value is correlated with the winding flux in the fault state. However, this element results in a change in impedance following the fault, which impacts on the switch's functionality. Ultimately the main branch connecting to the network has its current interruption when the DCCB current drops.

$$L_{11}.di/dt = V_{network} \quad (1)$$

$$R = \rho.l/A \quad (2)$$

$$L=\mu_0.\ \mu_r.A.N^2/l \quad (3)$$

III. Propose Controllable Saturated Core FCL

A. *General structure of CSCFCL*

Similar to PMFCL, general structure of CSCFCL consists of three primary components: a network coil, two numbers of permanent magnets in two yokes and an integrated ferrite core. The second and third coils are mounted on the limb of the right side of the core. The order of activation in the network for the second and third coils is shown in Fig. 4. General layout of CSCFCL and the network that connects to it are shown in Fig. 6-a. Through IGBT blocks and time-varying voltage sources, the control coils raise the network inductance and lower the fault current rate following the fault.

The primary coil that is linked to the grid is in the circuit and the core is saturated through PM before the fault occurs. An opposite flux to the PM flux is generated in the core when the fault occurs because the fault current rate increases. The desaturated core will be at point 1 as shown in Fig. 2 and move to point 2 as the fault current-induced flux exceeds the PM flux. The secondary coil is linked via the IGBT when the fault is detected by the current sensor. It generates an additional flux, which makes the core reach to the linear region in 2 more quickly than the saturation region in 1. This implies that the core depletes faster than expected. When the fault current is reduced temporarily due to an increase in the inductance, the current sensor recognizes it and quickly removes the second coil. (1) and (3) show that when the inductance is constant, it apears in the linear zone and lowers the fault current rate.

The fault flux is significant that it takes the core from the opposite side to point 3 in the saturation region after it has passed through the linear region. In this instance, the current sensor notices that the current slope has changed and is increased once more. Thus, by adding the third coil, the core is once more brought close to the linear region by producing a flux that matches the PM flux. This process repeats itself multiple times, with the third coil needing to produce more flux each time to overcome the incorrect current. It thus connects to a higher voltage level each time. The process's time sequence is depicted in Fig. 5. The maximum fault current and fault current rate are crucial factors in the FCL design. In this article, the creation of a control structure lowers the fault current rate and the maximum fault current.

Furthermore, the time control gives the core more time to lower the fault current, which lessens the stress on the DCCB as it decreases the fault current. However, the core's structure results in the main winding having fewer turns than PMFCLs, which, by (2), indicates that there are few in this instance. Then the current sensor notices that the current slope has changed and is now increasing once more. Thus, by adding the third coil, the core is once more brought close to the linear region by producing a flux that matches the PM flux. This process repeats itself multiple times, with the third coil needing to produce more flux each time to overcome the incorrect current. It thus connects to a higher voltage level each time. The process's time sequence is depicted in Fig. 5. The maximum fault current and fault current rate are crucial factors in the FCL design. In this article, the creation of a control structure lowers the fault current rate and the maximum fault current. Furthermore, the time control gives the core more time to lower the fault current, which lessens the stress on the DCCB as it decreases the fault current losses in the period preceding the fault in the network.

B. *Principle of CSCFCL*

As soon as the inductance momentarily decreases, the current sensor cuts off the secondary winding, and the fault current slope begins to decrease in the linear region between t_2 and t_3 due to the unsaturated core. By decreasing the inductance the current sensor detects in t_3, the third coil's circuit is activated, creating a flux in the core that is compatible with and opposed to the pm flux. The combined flux produced by the third coil and pm overcomes the fault flux and prevents Reduced inductance. The inductance is then moved from t_4 to

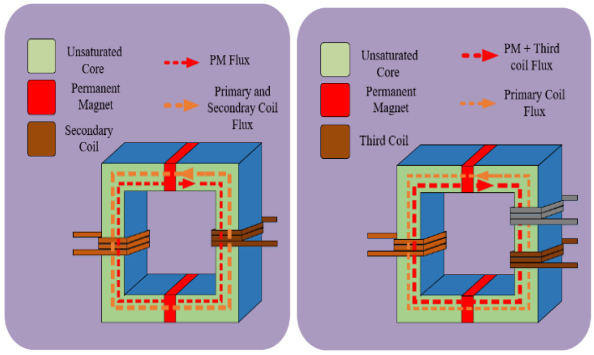

(a) (b)

Figure 4. (a)CSCFCL with secondary active winding (b)CSCFCL with third active winding

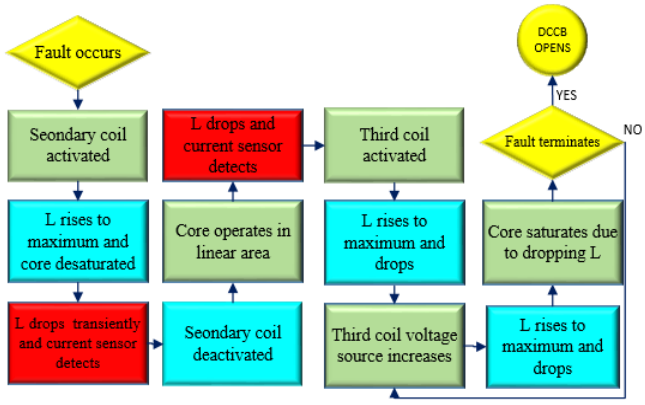

Figure 5. timing sequence of CSCFCL

t_5, which is close to the maximum inductance. Every cycle, as the inductance declines and the fault current slope climbs, the third coil consistently reaches a greater voltage level. As a result of the previously indicated third coil management, the fault current gradually decreases and the inductance profile in Fig. 1 approaches its maximum.

In addition to CSCFCL, Fig. 6-b depicts the magnetic equivalent circuit, and Fig. 6 illustrates the electric circuit of the DC network. Owing to the KCL (4) and (5), the value of inductance during the fault will be in (7), while in the state before the fault, when the core is at saturation, it is $\mu_{unsaturated} >> \mu_{saturated}$. It is derived from the (6) and the aforementioned equations. As the core moves away from saturation, the inductance rises according to (6), and the current falls according to (1).

As soon as the inductance momentarily decreases, the current sensor cuts off the secondary winding, and the fault current slope begins to decrease in the linear region between t_2 and t_3 due to the unsaturated core. By decreasing the inductance the current sensor detects in t_3, the third coil's circuit is activated, creating a flux in the core that is compatible with and opposed to the pm flux. The combined flux produced by the third coil and pm overcomes the fault flux and prevents Reduced inductance. The inductance is then moved from t_4 to t_5, which is close to the maximum inductance. Every cycle, as the inductance declines and the fault current slope climbs, the third coil consistently reaches a greater voltage level. As a result of the previously indicated third coil management, the fault current gradually decreases and the inductance profile in Fig. 1 approaches its maximum.

In addition to CSCFCL, Fig. 6-b depicts the magnetic equivalent circuit, and Fig. 6-a illustrates the electric circuit of the DC network. Owing to the KCL (4) and (5), the value of inductance during the fault will be in (7), while in the state before the fault, when the core is at saturation, it is $\mu_{unsaturated} >> \mu_{saturated}$. It is derived from the (6) and the aforementioned equations. As the core moves away from saturation, the inductance rises according to (6), and the current falls according to (1).

$$N_1 i_1 - H_c l_m + N_2 i_2 - N_3 i_3 = (R_{pm} + R_{core}) \cdot \varphi \quad (4)$$

$$L = N^2 / (R_{PM} + R_{core}) \quad (5)$$

$$L_{saturated} = 1 / [(l_{core} / \mu_s S_{core}) + (l_{pm} / \mu_{pm} S_{pm})] \quad (6)$$

$$L_{unsaturated} = 1 / (l_{pm} / \mu_{pm} S_{pm}) \quad (7)$$

Furthermore, we will observe changes in the voltage applied to the second and third windings, the impact on the fault current's slope and the length of the fault current's reduction by varying the number of turns of the control coils, N_2 and N_3. It is anticipated that when N_2 increases, the inductance will rise and the dominating flux of the core will decrease, As a result, the core takes a longer time to get out of saturation and the process of changing the slope of the fault current becomes slower. Additionally, it is anticipated that as V_2 increases, the fault current slope will likewise increase and it will take less time to achieve the maximum inductance per the equations (4) to (6).

The slope of the fault current will decrease when the third coil is introduced and the inductance is subsequently increased again, as we anticipate that raising V_3 will increase the flux in the direction of strengthening PM. The core will also extend the fault current reduction period by raising N_3. By altering the quantity We should be careful to ensure that the control coils and voltage level are adjusted so that the inductance profile has the biggest influence on the fault current slope.

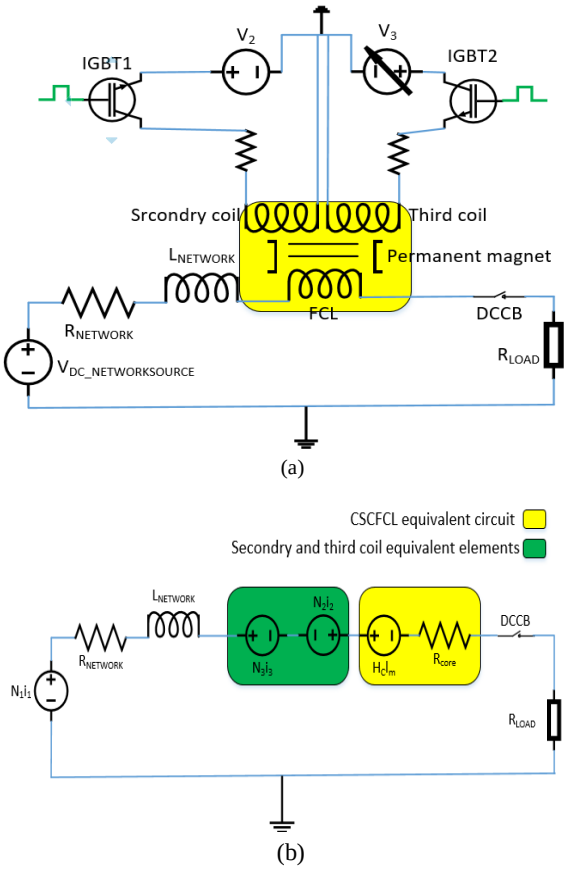

Figure 6. (a)CSCFCL structure (b)equivalent magnetic circuit of CSCFCL

IV. Simulation Results

As displayed in the Table I. The DCCB has a rated voltage of 1.5 kV and a fault current rise rate of 1.5 kA/ms. To check the sensitivity of the situation, the procedure of altering the secondary coil's voltage level to examine variations in inductance and current was carried out in Table I. Furthermore, when a fault occurs, the third coil is activated with two steps of different voltage levels; in this scenario, first voltage level is set and the second voltage level is examined. The secondary coil has very little effect on the third coil. As a result, the third coil is added to the analyzed results once the secondary coil has been changed.

Table I. CSCFCL specification

Nominal voltage	1.5 kV
Nominal current	1 kA
Rise Rate of fault current	1.5 kA/ms
Maximum fault current	12 kA

A. Sensitivity of control voltage of Secondary winding

To increase the core's speed desaturation, the secondary coil is intended. Fig. 7-a shows that the time it takes to attain saturation increases with the secondary coil's voltage level when its number of turns is set at 10. The core flux tends to bring the core to saturation, and it has gotten faster since hitting the 2 kV voltage threshold. To put it another way, the high voltage level applied to the secondary winding causes the core to go through saturation twice before reaching the linear region and then again after 0.5 ms, which is not expected. However, it does so more quickly and ultimately overcomes the PM flux.

However, if the dominating flux caused by PM is high as shown in Fig. 8-b the fault current's slope would increase excessively, and the fault's unstable condition will not be improved.

The core is faster than saturation when the voltage level reaches 1 kV, however, the fault current rate does not appear to decrease. The inductance profile has reached the linear zone at an acceptable speed by providing a voltage of 1.5 kV, and the core enters the linear region at a faster rate by roughly 0.5 ms. This is seen in Fig. 8-a about the inductance PMFCL slope.

When applying a voltage of 1.5 kV showed in Fig. 7-b, the slope of the core fault current is lower than other applied voltages. Additionally, by comparing the slope of PMFCL current in Fig .8-b, it can be seen that, at t=15 ms, the value of PMFCL current was around 9.8 kA. However; this value was lowered to 9.3 kA upon the application of the secondary winding.Additionally, by comparing the slope of PMFCL current in Fig. 8-b, it can be seen that, at t=15 ms, the value of PMFCL

The current was around 9.8 kA; however, this value was lowered to 9.3 kA upon the application of the secondary winding.

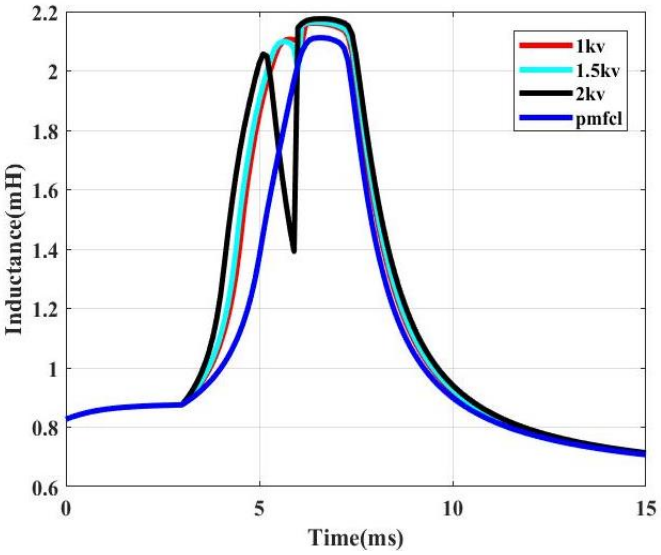

(a)

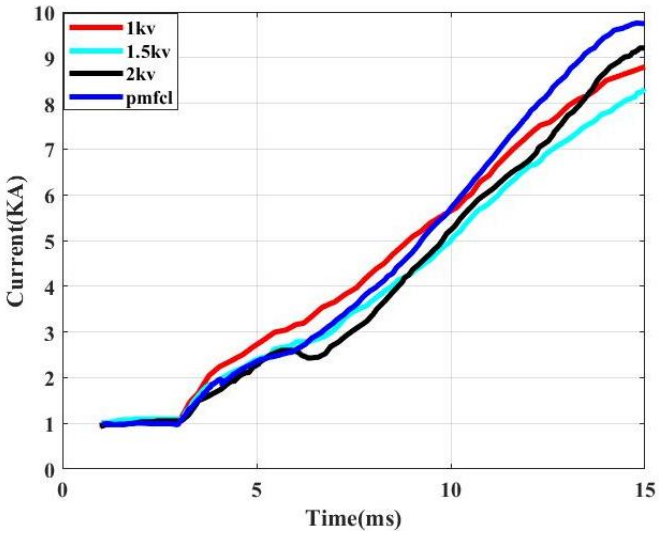

(b)

Figure 7. (a)Secondary winding inductance of CSCFCL and PMFCL (b)Secondary and Third windings current of CSCFCL and PMFCL

B. Sensitivity of control voltage of Third winding

The applied primary voltage is determined to be 5 kV. By setting the secondary winding voltage in the preceding section, the third winding voltage has been set as shown in Table II. The applied primary voltage of around 0.4 ms is deemed appropriate based on the inductance profile and simulations since it maintains the inductance in the linear zone following the inductance drop. Subsequently, a larger voltage is applied to the third winding by raising the fault flux.

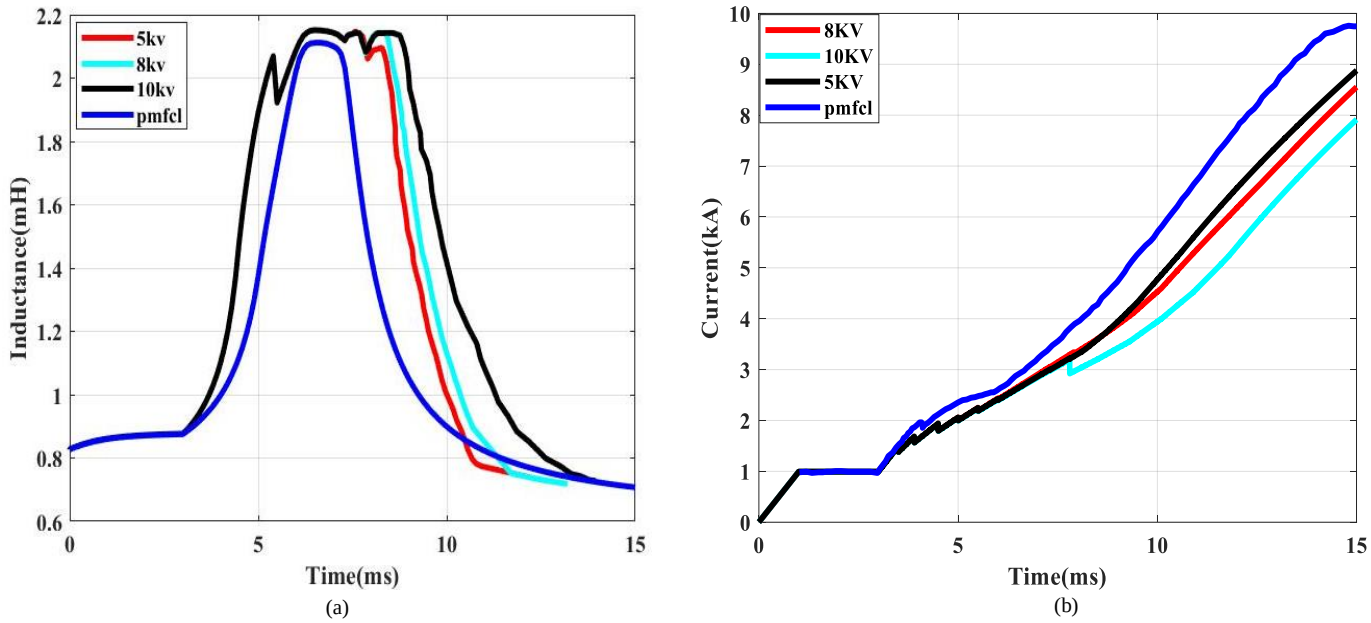

(a) (b)

Figure 8. (a)Secondary and Third windings inductance of CSCFCL and PMFCL(b)Secondary and Third windings current of CSCFCL and PMFCL

Table II shows that when the voltage is increased, the inductance experiences a brief dip before returning to the linear zone, which keeps the value of the current slope near the initial value.

The inductance rose in the second step of applying voltage to the third winding, as shown in Fig. 8-a. This indicates that the core can re-enter the linear area with a limited rise in voltage based on the number of fixed turns. The inductance was in the linear region for 0.7 ms and then returned to the saturated region, as shown in Fig. 8-a. By providing a voltage of 10 kV in the second step. The current diagram with the second and third coils applied is displayed in Fig. 8-b. The application of all three voltage is evident. In comparison to PMFCL, the third winding has resulted in a 1.5 kA reduction in current and a 24% decrease in current slope.

Table II. CSCFCL windings voltage specification

	Number of turns	Sec winding voltage	Third winding step1	Third winding step2
1	10	1500 V	5kV	5kV
2	10	1500 V	5kV	8kV
3	10	1500 V	5kV	10kV

V. Comparison Study

The advantages of CSCFCLs over PMFCLs are as follows:

1) Controllability: It is evident from the data that the main benefit of CSCFCLs over PMFCL fault current limiters is their controllability. The amount and rate of current are directly lowered by the speed at which an object enters and exits the saturation zone from the core, as indicated by the equations in the preceding sections. While CSCFCL is far more versatile and customizable than PMFCL, there is a fault because of the use of auxiliary windings in this model.

2) Complexity: Regardless of the core material, the dimensions of the core in CSCFCL are significantly smaller than in PMFCL, and just two windings are added to the core structure. This reduces complexity in the core structure.

3) Core loss: Loss is smaller in the CSCFCL than the other PMFCLs because of the smaller core's volume and in pre-fault state the primary coil has fewer turns that connected to the network. Thus, the decrease in the present rate in the CSCFCL with The primary winding has fewer turns than PMFCL, and number of turns in the secondary and third windings are changed.

4) Flexibility: The restrictions of establishing DCCB and other parts in the DC network can be lessened by using CSCFCL in various networks because of its flexibility in reducing the fault current rate. This allows for the creation of broader networks.

The comparison between PMFCL and CSCFCL is displayed in Table III:

Table III. Comparison between PMFCL and CSCFCL

structure	PMFCL	CSCFCL
Controllability	Low	High
Complexity	Average	Low
Core Loss	Average	Low
Flexibility	Average	High

VI. Conclusion

This article proposed a structure based on time control and FCL structure enhancement, using the CSCFCL structure instead of the PMFCL structure. Lack of temporal controllability was one of PMFCL's shortcomings which was addressed in CSCFCL with two control windings and control circuits. As mentioned previously control winding extended the time that the CSCFCL worked in the linear zone, which decreased the fault current and its slope. The limitation of producing DCCB and other parts in the DC network can be resolve by using CSCFCL in various networks because of its flexibility in reducing the fault current rate. This allows for the creation of wider networks. Furthermore, the decrease in the size of the network's core and the quantity of turns in the winding resulted in the pre-fault state, there will be a reduction in the core and network losses. By using control winding, the fault current slope in CSCFCL was decreased by approximately 25 % in comparison to PMFCL, and the fault current's overall slope was lowered by approximately 40 %. The finite element simulation results verified the validity of the proposed design.

References

[1] O. Gomis-Bellmunt, J. Liang, J. Ekanayake, R. King, and N. Jenkins, "Topologies of multiterminal HVDC-VSC transmission for large offshore wind farms," Electric Power Systems Research, vol. 81, no. 2, pp. 271–281, Feb. 2011, doi: 10.1016/j.epsr.2010.09.006.

[2] Faculty of Engineering at Helwan - Helwan University and S. Hasan, "A hybrid circuit breaker based on current commutation approach for multi feeders DC railway substations," CSEE JPES, May 2019, doi: 10.17775/CSEEJPES.2017.00290.

[3] Hengxu Ha, S. Subramanian, A. Dysko, S. Ademi, D. Vozikis, and D. Tzelepis, "Impact of VSC converter topology on fault characteristics in HVDC transmission systems," in 8th IET International Conference on Power Electronics, Machines and Drives (PEMD 2016), Glasgow, UK: Institution of Engineering and Technology, 2016, p. 6 .-6 . doi: 10.1049/cp.2016.0263.

[4] H. Chen, J. Yuan, H. Zhou, S. Xu, C. Zou, and F. Chen, "A Novel Fast Energy Storage Fault Current Limiter Topology for High-Voltage Direct Current Transmission System," IEEE Trans. Power Electron., vol. 37, no. 5, pp. 5032–5046, May 2022, doi: 10.1109/TPEL.2021.3110274.

[5] C. Li, X. Bie, W. Ma, X. Liu, and X. Guo, "Study on Control and Protection Strategy of Neutral Bus Switch in HVDC Flexible Transmission System," in 2019 4th IEEE Workshop on the Electronic Grid (eGRID), Xiamen, China: IEEE, Nov. 2019, pp. 1–4. doi: 10.1109/eGRID48402.2019.9092679.

[6] Z. Wang et al., "Optimal Design of 535kV High Speed Mechanical Switch Pin Based on MAXWELL and LS-DYNA," in 2019 IEEE Innovative Smart Grid Technologies - Asia (ISGT Asia), Chengdu, China: IEEE, May 2019, pp. 960–963. doi: 10.1109/ISGT-Asia.2019.8881377.

[7] D. Qin, Y. Chen, Z. Zhang, and J. Enslin, "A Hierarchical Microgrid Protection Scheme using Hybrid Breakers," in 2021 IEEE 12th International Symposium on Power Electronics for Distributed Generation Systems (PEDG), Chicago, IL, USA: IEEE, Jun. 2021, pp. 1–6. doi: 10.1109/PEDG51384.2021.9494192.

[8] S. Kamtip and K. Bhumkittipich, "Comparison between mechanical circuit breaker and solid state circuit breaker under abnormal conditions for low voltage systems," in 2015 18th International Conference on Electrical Machines and Systems (ICEMS), Pattaya, Thailand: IEEE, Oct. 2015, pp. 1091–1096. doi: 10.1109/ICEMS.2015.7385200.

[9] S. Rahimpour, O. Husev, and D. Vinnikov, "Impedance-Source DC Solid-State Circuit Breakers: An Overview," in 2022 International Symposium on Power Electronics, Electrical Drives, Automation and Motion (SPEEDAM), Sorrento, Italy: IEEE, Jun. 2022, pp. 186–191. doi: 10.1109/SPEEDAM53979.2022.9842138.

[10] S. Moury, J. Lam, V. Srivastava, and R. Church, "A novel multi-input converter using soft-switched single-switch input modules with integrated power factor correction capability for hybrid renewable energy systems," in 2016 IEEE Applied Power Electronics Conference and Exposition (APEC), Long Beach, CA, USA: IEEE, Mar. 2016, pp. 786–793. doi: 10.1109/APEC.2016.7467961.

[11] Y. Han, D. Lin, T. Yaxiong, and W. Xueguang, "Transient Characteristic Parameters Monitoring and Diagnosis of the Hybrid HVDC Circuit Breaker," in 2018 IEEE International Conference on High Voltage Engineering and Application (ICHVE), ATHENS, Greece: IEEE, Sep. 2018, pp. 1–4. doi: 10.1109/ICHVE.2018.8642194.

[12] M. A. Ahmed, T. Messo, P. Rasilo, and J. Rekola, "Dynamic modelling of grid-connected permanent magnet synchronous generator wind turbine: rectifier dynamics and control design," J. eng., vol. 2019, no. 18, pp. 5202–5207, Jul. 2019, doi: 10.1049/joe.2018.9343.

[13] IEEE PC57.16/D9, January - April 2011: IEEE Draft Standard Requirements, Terminology, and Test Code for Dry-Type Air-Core Series-Connected Reactors. Place of publication not identified: IEEE, 2011.

[14] PC37.302/D3, August 2015 - IEEE Draft Guide for Fault Current Limiter (FCL) Testing FCLs rated above 1000 V AC. Place of publication not identified: IEEE, 2015.

[15] M. Mousa, M. Babaei, and S. Abdelwahed, "A novel sensitivity analysis for optimal design of superconductive fault current limiter in microgrids," Electr Eng, vol. 103, no. 1, pp. 479–491, Feb. 2021, doi: 10.1007/s00202-020-01086-4.

[16] W. T. Norris and A. Power, "Fault current limiters using superconductors," Cryogenics, vol. 37, no. 10, pp. 657–665, Jan. 1997, doi: 10.1016/S0011-2275(97)00059-3.

[17] D. Cvoric, S. W. H. De Haan, and B. Ferreira, "CB stress reduction and comparison of energy dissipation for two types of FCLs," in 2008 IEEE/PES Transmission and Distribution Conference and Exposition, Chicago, IL, USA: IEEE, Apr. 2008, pp. 1–7. doi: 10.1109/TDC.2008.4517214.

[18] S. Farhadkhani, J. Lobry, F. Vallee, and O. Durieux, "Investigating the Characteristics and Effects of FCLs on Distribution Grids with Wind Generation," in 2014 IEEE Electrical Power and Energy Conference, Calgary, AB, Canada: IEEE, Nov. 2014, pp. 65–70. doi: 10.1109/EPEC.2014.32.

[19] B. Shen, J. Yang, M. Tian, and T. Coombs, "Saturated Iron-core Superconducting Fault Current Limiter for VSC Network: System Modeling With Loss Analysis," IEEE Trans. Appl. Supercond., vol. 31, no. 8, pp. 1–4, Nov. 2021, doi: 10.1109/TASC.2021.3094448.

[20] A. Jafari, S. Mohsenzade, and A. A. Razi-Kazemi, "Controllable DC Fault Current Limiter with Loss Reduction," in 2023 14th Power Electronics, Drive Systems, and Technologies Conference (PEDSTC), Babol, Iran, Islamic Republic of: IEEE, Jan. 2023, pp. 1–5. doi: 10.1109/PEDSTC57673.2023.10087155.